INTERNATIONAL JOURNAL FOR NUMERICAL METHODS IN FLUIDS
Int. J. Numer. Meth. Fluids 2009; **61**:752–767
Published online 9 January 2009 in Wiley InterScience (www.interscience.wiley.com). DOI: 10.1002/fld.1977

A confrontation of 1D and 2D RKDG numerical simulation of transitional flow at open-channel junction

R. Ghostine[1,*,†], G. Kesserwani[1], R. Mosé[1], J. Vazquez[1], A. Ghenaim[2] and C. Grégoire[3]

[1]*IMFS, UMR 7507 UDS-ENGEES-CNRS, 2 rue Boussingault, 67000 Strasbourg, France*
[2]*INSA de Strasbourg, 24 boulevard de la Victoire, 67084 Strasbourg cedex, France*
[3]*LHYGES, UMR 7517 UDS-ENGEES-CNRS, 1 rue Blessig, 67084 Strasbourg cedex, France*

SUMMARY

In this study, a comparison between the 1D and 2D numerical simulation of transitional flow in open-channel networks is presented and completely described allowing for a full comprehension of the modeling water flow. For flow in an open-channel network, mutual effects exist among the channel branches joining at a junction. Therefore, for the 1D study, the whole system (branches and junction) cannot be treated individually. The 1D Saint Venant equations calculating the flow in the branches are then supplemented by various equations used at the junction: a discharge flow conservation equation between the branches arriving and leaving the junction, and a momentum or energy conservation equation. The disadvantages of the 1D study are that the equations used at the junction are of empirical nature due to certain parameters given by experimental results and moreover they often present a reduced field of validity. On the contrary, for the 2D study, the entire network is considered as a single unit and the flow in all the branches and junctions is solved simultaneously. Therefore, we simply apply the 2D Saint Venant equations, which are solved by a second-order Runge–Kutta discontinuous Galerkin method. Finally, the experimental results obtained by Hager are used to validate and to compare the two approaches 1D and 2D. Copyright © 2009 John Wiley & Sons, Ltd.

Received 29 May 2008; Revised 14 October 2008; Accepted 8 November 2008

KEY WORDS: open channel junctions; Saint Venant equations; discontinuous Galerkin method; momentum conservation; transitional flow; steady flow

1. INTRODUCTION

The junction of two open channels is a common occurrence in many hydraulic structures ranging from wastewater treatment facilities to fish passage conveyance structures. While open-channel

*Correspondence to: R. Ghostine, Systèmes Hydrauliques Urbains, Ecole Nationale du Génie de l'Eau et de l'Environnement de Strasbourg, France.
†E-mail: rabih.ghostine@engees.u-strasbg.fr

junctions are present in many hydraulic systems, only limited research has been conducted on the topic. In recent years more focus has been given to the combining open-channel junction problem. Prior studies have focused on simplified 1D mathematical approximation of different junction flow characteristics with limited data collected to validate the theoretical models.

The difficulty in addressing the problem theoretically is that there are numerous factors that influence flow characteristics at the junction of two open channels. One set of variables can be described as geometry variables, such as the size, shape, slope, and angle between the combining branches. Many combinations of these four variables are possible. A second set are flow variables, such as the Froude number in the downstream flow, the channel roughness, the ratio of discharge between the two tributary branches, and the variation of fluid properties. It is readily apparent that a simplified 1D mathematical model is incapable of fully describing the complex flow conditions present at a junction. The difficulty of adequately describing this flow with simplified mathematical models leads to the possibility of using a 2D code to describe the flow conditions in a combining open-channel junction.

In this work, we simulate and compare the 1D approach with the numerical results obtained by the 2D Saint Venant equations. For the 1D study, the presence of internal junctions in such a system poses difficulties in numerical solution and routing of unsteady flow through the system because these junctions act as internal boundary conditions for each channel joined at the junction [1]. Therefore, 1D flow simulation in open-channel network is much more complicated than single channel solutions, especially for large-scale network systems [2, 3]. The whole system is considered as a set of branches in which the 1D Saint Venant equations are applied and linked by different hydraulic models of junction. The hydraulic conditions at a junction can be modeled by the mass conservation equation and either the energy conservation equation or the momentum equation. In this work, we use the model developed by Gurram [4]. While for the 2D case, the whole system (branches and junction) is considered as one system and discretized into triangular cells forming an unstructured computational mesh. Therefore, we simply apply the 2D Saint Venant equations, which are solved by a second-order Runge–Kutta discontinuous Galerkin (RKDG) method [5–7]. The experimental results obtained by Hirsh [8] are used to validate and to compare the two approaches 1D and 2D in simulation of transitional steady flow through the combining junction.

The objective of this paper is to show that the 1D approximation is not acceptable in all cases and that with a 2D approach we can obtain very accurate results with a reasonable space discretization and therefore a reasonable CPU time.

The organization of this paper is as follows. In Section 2, we present the review of literature. In Sections 3 and 4, we describe in detail the equations and the numerical methods used for the two approaches 1D and 2D. In Section 5, we provide numerical examples to compare the two approaches. Concluding remarks are given in Section 6.

2. REVIEW OF LITERATURE

Previous studies on combining open-channel flows proposed theoretical approaches based on the mass and momentum conservation for determining the upstream-to-downstream depth ratio. Taylor [9] presented the first study on junction flow and referred to the complexity of the problem. He

DOI: 10.1002/fld

conducted experiments in horizontal rectangular channels of junction angles 45 and 135°. For a given downstream flow depth h_d and upstream-to-downstream discharge ratio $q = Q_u/Q_d$, he derived an equation for the relative upstream flow depth $Y = h_u/h_d$. A comparison with data showed fair agreement for $\delta = 45°$ and poor agreement for $\delta = 135°$. A second systematic study on junction flow was presented by Webber and Greated [10]. A small model with junction angles $\delta = 30°$, $\delta = 60°$, and $\delta = 90°$ was used. Modi *et al.* [11] investigated open-channel junction using conformal mapping (based on a complex variable theory) and therefore did not take into account energy losses. Best and Reid [12] analyzed experimentally the geometry of the separation zone at sharp-edged open-channel junctions. The results included data for the length and the maximum width of the separation zone. They found that both the width and length of the separation zone increase with an increase in junction angle and discharge of the lateral channel. The shape index of the separation zone was defined as the ratio of the maximum recirculation width and its length. For a right-angled junction flow, the shape index has approximately the same value for various discharge ratios with a mean value of 0.19. By discussing the experimental approach of Best and Reid [12], Hager [13] introduced a simple model in which the pressure distribution on the lateral sidewall and the lateral momentum contribution were taken into account. He aimed at predicting the width of the separation zone by a 1D approach. Ramamurthy *et al.* [14] studied combining open-channel flow at right-angled junction based on the momentum transfer from the lateral to main branch. He applied separate momentum equations for the flow in the lateral and main channels. The lateral momentum contribution was found to increase as the lateral discharge ratio increases. Gurram *et al.* [15] studied the characteristics of the lateral flow and the flow contraction in the tail water channel and determined expressions for the momentum correction coefficient and the lateral wall pressure force. An equation for the ratio of flow depths in the lateral and upstream branches was also provided. Hsu *et al.* [16, 17] applied overall mass and energy conservation to the junction and momentum conservation to two control volumes in the junction and computed an energy loss coefficient and the depth ratio. All these studies were for equal-width junction flows and equality of the upstream flow depths was assumed. Recently, Shabayek *et al.* [18] developed a 1D model providing the necessary internal boundary equations for combining subcritical open-channel junctions. The advantage of this model is that it does not assume equal upstream flow depths. The model is based on the momentum principle together with mass continuity through the junction.

Very few studies concerning the problem of the junction in the transitional case is found. Ramamurthy *et al.* [14] studied the two types of flow, subcritical and transitional, through a junction for a right-angled junction. The model of junction developed in this work is based on the conservation of the momentum of the lateral branch to the main channel. It separately applied the equations of the momentum for the flow in the lateral and upstream branches.

Hager [19] showed that the transitional flow can exist if the discharge lateral flow is at least equal to 15% of the total flow. The author carried out a detailed experimental study with a 1D theoretical analysis of the transitional flow with angles of junction equal to 90, 45 , and 22.5°. Hager derived an equation for the coefficient of contraction of the zone of separation. The author thus developed a model for the junction defining the water depths ratio at the junction, as a function of the flow discharge and the junction angle. The experimental validation of this model was less satisfactory for an angle of junction equal to 90° than for the other angles.

Gurram [4] proved that certain assumptions considered by Hager are not acceptable, and he developed a model for the junction which reproduces more accurately the experimental results of Hager [19].

DOI: 10.1002/fld

3. 1D STUDY

It is well known that the 1D Saint Venant equations are not available at the points enclosing the junction due to the 2D phenomenon of the junction. Therefore, for the 1D study, the junction acts as an internal boundary condition and a special treatment is necessary. To find the solution in a network system, the 1D Saint Venant equations are applied in branches and linked by a junction model based on momentum or energy conservation. Different junction models are developed in the literature to relate the different flow variables at the junction. The inconvenience of these models is that they are of empirical nature due to certain parameters given by the experimental results and they often present a reduced field of validity. For example, they are developed in case of subcritical or transitional or supercritical flow and for a network system composed of three rectangular branches linked by one combining junction.

3.1. 1D junction model

To describe briefly the 1D junction model used in this work, let us consider a network system composed of three rectangular branches of same width B and linked by one combining junction. We note by branch u, branch L and branch d, the main channel located before the junction, the lateral channel branching to the main channel and the main channel located after the junction, respectively (Figure 1). The water depths and discharges at the upstream, lateral and downstream points to the junction are denoted by h_{u}, h_L, h_{d}, Q_{u}, Q_L and Q_{d}. The junction angle is denoted by δ.

The developed model for transitional flow junction and used in this work is Gurram's model [15]. This model assumes the equality of the water depth in the upstream branches and critical flow at the entrance of the downstream branch.

The model derived by Gurram *et al.* [15] is:

$$\begin{aligned} h_{\mathrm{u}} &= h_L \\ Y^3 - 3Y + 2[q^2 + (1-q)\cos\delta] &= 0 \end{aligned} \tag{1}$$

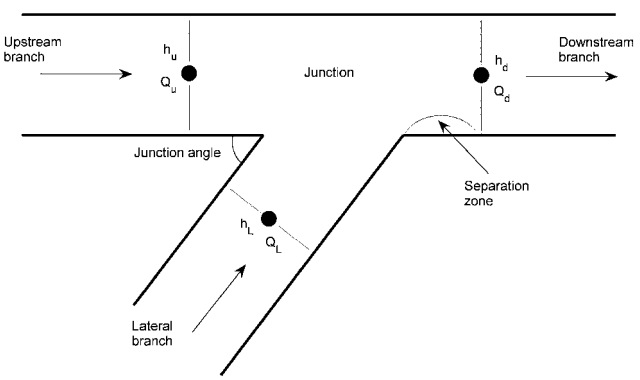

Figure 1. 1D junction problem.

DOI: 10.1002/fld

3.2. Coupling the channel solution with the junction model

To find the solution at the internal points enclosing the junction, we have to find six unknown variables: the water depths and the flow discharges at the downstream of the branches located before the junction, the water depth and the flow discharge at the upstream of the branch located after the junction (Figure 1). Therefore, we need six equations to solve the 1D junction problem.

Since the flow is subcritical in the upstream branches, only two equations come from the branches' solutions through the characteristic equations. These equations relate the flow discharge as a function of the water depth:

$$\begin{aligned} Q_{\mathrm{u}} &= f_{\mathrm{u}}(h_{\mathrm{u}}) \\ Q_L &= f_L(h_L) \end{aligned} \tag{2}$$

For more information about the method of characteristics, see [8].

The conservation of mass gives at the junction is given as follows:

$$Q_{\mathrm{u}} + Q_L = Q_{\mathrm{d}} \tag{3}$$

Critical flow at the entrance of the downstream branch indicates that the downstream Froude number is equal to 1:

$$\frac{Q_{\mathrm{d}}^2}{gB^2h_{\mathrm{d}}^3} = 1 \tag{4}$$

The last two equations come from the model quoted above (Equation (1)).

The system of these six equations is non-linear and its resolution is obtained by a Newton–Raphson method.

4. 2D STUDY

4.1. 2D Saint Venant equations

The unsteady, 2D Saint Venant equations can be written in the following conservative form as:

$$\frac{\partial U}{\partial t} + \frac{\partial E}{\partial x} + \frac{\partial G}{\partial y} = S \tag{5}$$

in which

$$U = \begin{pmatrix} h \\ hu \\ hv \end{pmatrix}, \quad E = \begin{pmatrix} hu \\ hu^2 + gh^2/2 \\ huv \end{pmatrix}, \quad G = \begin{pmatrix} hv \\ huv \\ hv^2 + gh^2/2 \end{pmatrix}$$

and

$$S = S_0 + S_f = \begin{pmatrix} 0 \\ ghS_{0x} \\ ghS_{0y} \end{pmatrix} + \begin{pmatrix} 0 \\ -ghS_{fx} \\ -ghS_{fy} \end{pmatrix} \text{ is the source term}$$

DOI: 10.1002/fld

where u and v are the velocity components in the x and y directions, respectively; h is the water depth; g is the acceleration due to gravity; (S_{0x}, S_{0y}) are the bed slopes in the x and y directions and (S_{fx}, S_{fy}) are the friction slopes in the x and y directions, respectively. In this study, the friction slopes are estimated by using Manning's formula:

$$S_{fx} = \frac{n_{\mathrm{M}}^2 u\sqrt{u^2+v^2}}{h^{4/3}}, \quad S_{fy} = \frac{n_{\mathrm{M}}^2 v\sqrt{u^2+v^2}}{h^{4/3}}$$

where n_{M} is Manning's roughness coefficient. In our work, as we are in a rough turbulent flow, the viscosity (turbulence) and the bed roughness are approximated by the empirical Manning formula with Manning's roughness coefficient n_{M}.

4.2. Numerical method

The DG finite element formulation is written for each element K. Equation (5) is first multiplied with test function $v_h(x, y)$ and the flux integrals are further integrated by parts. The whole process yields:

$$\begin{aligned}\frac{\mathrm{d}}{\mathrm{d}t}\int_K U_h(x,y,t)v_h(x,y)\,\mathrm{d}K &= \int_K F(U_h(x,y,t))\cdot\nabla v_h(x,y)\,\mathrm{d}K \\ &\quad - \int_{\partial K} F(U_h(x,y,t))\cdot n_k v_h(x,y)\,\mathrm{d}\Gamma \\ &\quad + \int_K S(U_h(x,y,t))v_h(x,y)\,\mathrm{d}K \end{aligned} \tag{6}$$

where $F = (E, G)$ and $n_k = (n_x, n_y)$ is the outward unit normal of the element boundary surface.

In this paper, linear triangular elements are used to discretize the 2D spatial domain. Hence, the solution at any point in each element can be represented in terms of the midpoint solutions U_i and the shape functions φ_i at each midpoint:

$$U_h(x, y) = \sum_i U_i \varphi_i(x, y) \tag{7}$$

Using the standard Galerkin approach, shape functions and test functions are identical. Rewriting Equation (6), the discontinuous Galerkin space discretization can be summarized by a system of ordinary differential equations as follows:

$$\frac{\mathrm{d}}{\mathrm{d}t} M U_h = L_{h,U}(U_h) \tag{8}$$

where M is the mass matrix and L_h is an operator describing the spatial discretization.

By using orthogonal shape functions, the mass matrix M in the linear equation system (8) becomes diagonal. For triangular elements, a linear shape function can be obtained by choosing a function that takes the value of 1 at the midpoint m_i of the ith edge of a triangle, and the value of 0 at the midpoints of the other two edges. Thus, the diagonal mass matrix can be expressed as follows:

$$M = |K|\,\mathrm{diag}(\tfrac{1}{3}, \tfrac{1}{3}, \tfrac{1}{3}) \tag{9}$$

The integrals are approximated by a three-midpoint rule for the triangles and a two-point Gauss integration for the line integrals [18].

DOI: 10.1002/fld

4.3. Numerical flux

The approximation of the numerical flux for the discontinuous Galerkin method is identical to the approximated solution of a Riemann problem according to finite-volume methods. By using linear or higher subcell resolution for higher-order discontinuous Galerkin methods, the scheme gets less sensitive to the choice of the numerical flux than the Godunov [20] type methods. In that case, a simple Lax–Friedrich flux gives good results.

$$F(U_L, U_R)\cdot n = \tfrac{1}{2}[(F(U_L)+F(U_R))\cdot n - a_{\max}(U_R - U_L)] \tag{10}$$

where $a_{\max} = \max(|a^1|, |a^2|, |a^3|)$, and a^k $(k=1,\ldots,3)$ are the eigenvalues of the Jacobian matrix:

$$\widetilde{A} = \frac{\partial(F\cdot n)}{\partial U} = \begin{bmatrix} 0 & n_x & n_y \\ (c^2-u^2)n_x - uvn_y & 2un_x + vn_y & un_y \\ (c^2-u^2)n_y - uvn_x & vn_x & un_x + 2vn_y \end{bmatrix}$$

and $c=\sqrt{gh}$ is the wave celerity.

4.4. Slope limiter

The following slope limiter is presented for a scalar quantity u_h. Its extension to systems is outlined. For further information, see Cockburn and Shu [5]. To describe the limiter, we use the same notations as in Cockburn and Shu [5]. For an arbitrary triangle K_0 and its surrounding neighbors K_i, $i=1,\ldots,3$, the notations b_i, $i=0,\ldots,3$, and m_i, $i=1,\ldots,3$, refer, respectively, to the barycenters of the triangles and the midpoints of the edges within K_0 (Figure 2).

Choosing any edge midpoint m_1, we obtain:

$$m_1 - b_0 = \alpha_1(b_1 - b_0) + \alpha_2(b_2 - b_0) \quad \text{for some } \alpha_1, \alpha_2 \in R^{+^2} \tag{11}$$

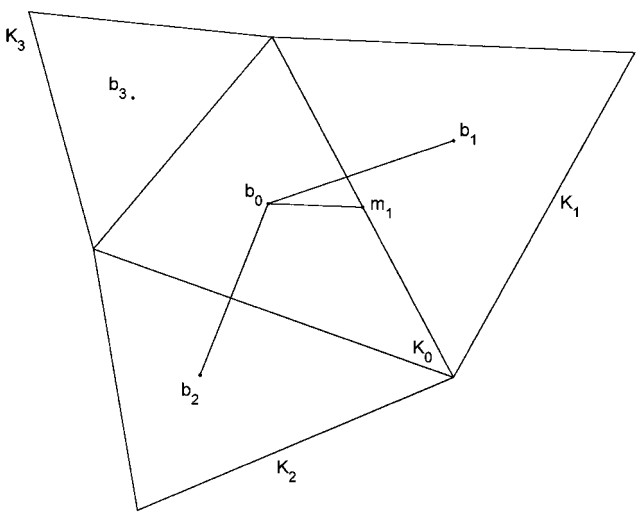

Figure 2. Slope limiting for triangular elements.

DOI: 10.1002/fld

For any linear function u_h, the mean gradient can be expressed as:

$$\Delta\overline{u}(m_1, K_0) = \alpha_1(u_h(b_1) - u_h(b_0)) + \alpha_2(u_h(b_2) - u_h(b_0)) \tag{12}$$

By using the basis functions φ_i, u_h can be expressed over K_0 as follows:

$$u_h(x, y) = \sum_{i=1}^{3} u_h(m_i)\varphi_i(x, y) = u_h(b_0) + \sum_{i=1}^{3} (u_h(m_i) - u_h(b_0))\varphi_i(x, y) \tag{13}$$

First, we compute the quantities:

$$\Delta_i = \widetilde{m}(u_h(m_i) - u_h(b_0), \nu\Delta\overline{u}(m_i, K_0)) \quad \text{for some } \nu > 1 \tag{14}$$

where ν is a positive constant number equal to 1.5 and $\widetilde{m}$ is the TVB minmod function defined as follows:

$$\widetilde{m}(a_1, a_2) = \begin{cases} a_1 & \text{if } |a_1| \leqslant M(\Delta x)^2 \\ m(a_1, a_2) & \text{otherwise} \end{cases} \tag{15}$$

where M is a given positive constant; and m is the minmod function, defined as follows:

$$m(a_1, a_2) = \begin{cases} s \min\limits_{1 \leqslant n \leqslant 2} |a_n| & \text{if } s = \text{sign}(a_1) = \text{sign}(a_2) \\ 0 & \text{otherwise} \end{cases} \tag{16}$$

Consequently, reconstruction is carried out according to the following two cases:

1. If $\sum_{i=1}^{3} \Delta_i = 0$, the new midpoint value is given by:

$$u_h(m_i) = u_h(b_0) + \sum_{i=1}^{3} \Delta_i \varphi_i(x, y) \tag{17}$$

2. If $\sum_{i=1}^{3} \Delta_i \neq 0$, we compute:

$$\text{pos} = \sum_{i=1}^{3} \max(0, \Delta_i), \quad \text{neg} = \sum_{i=1}^{3} \max(0, -\Delta_i) \tag{18}$$

and define:

$$\theta^+ = \min\left(1, \frac{\text{neg}}{\text{pos}}\right), \quad \theta^- = \min\left(1, \frac{\text{pos}}{\text{neg}}\right) \tag{19}$$

Finally, the new midpoint value is given by:

$$u_h(m_i) = u_h(b_0) + \sum_{i=1}^{3} \widehat{\Delta}_i \varphi_i(x, y) \tag{20}$$

where

$$\widehat{\Delta}_i = \theta^+ \max(0, \Delta_i) - \theta^- \max(0, -\Delta_i) \tag{21}$$

DOI: 10.1002/fld

Since the shallow water equations are a system of equations, the limiting must be performed in the local characteristic variables in the direction of the vector $m_1 - b_0$. The variables are therefore transformed by T^{-1} into the characteristic space, where T is the matrix of right eigenvectors of the following Jacobian:

$$\partial_U(E(U(b_0)), G(U(b_0))) \cdot \frac{m_i - b_0}{|m_i - b_0|} \tag{22}$$

4.5. Time integration

The second-order accurate two-stage TVD Runge–Kutta schemes of Cockburn and Shu [5] is employed in this work. According to Cockburn and Shu [5], the optimal two-stage, second-order accurate TVD Runge–Kutta scheme is expressed as:

$$\begin{aligned} U_h^1 &= U_h^n + \Delta t \cdot L_{h,U}(U_h^n) \\ U_h^{n+1} &= \tfrac{1}{2}(U_h^n + U_h^1 + \Delta t \cdot L_{h,U}(U_h^1)) \end{aligned} \tag{23}$$

The time step for a 2D element i is determined according to [RKDG formulation], namely,

$$\Delta t = \mathrm{CFL} \frac{|K_i|}{\sum_{j=1}^{3} l_j \min(u \cdot n_x + v \cdot n_y - c, 0)} \tag{24}$$

Here u, v and c are evaluated at the barycenter of the element, j is the index of the faces surrounding the element, l_j is the length of the face and $0 < \mathrm{CFL} \leqslant 1$ is the Courant number.

5. NUMERICAL RESULTS

In this section, we present the results of our numerical simulation of transitional flow at a combining junction obtained by the two approaches 1D and 2D. For the 1D simulation, we use the 1D Saint Venant equations in branches and linked by Gurram's model [4], the characteristics equations and the conservation of the flow discharge equation to calculate the flow variables at the junction (Figure 3). Oppositely, for the 2D simulation, the whole system (branches and junction) is considered as one system and we simply apply the 2D Saint Venant equations on unstructured triangular grids (Figure 4). Therefore, these equations do not require complementary equations to treat the junction as it is in the 1D case.

The experimental data obtained by Hager [19] will be compared with the computational results obtained by the two approaches. The data were analyzed, and information was developed that provides guidance for the design of open channel junctions with transitional flows. The 1D and 2D approaches were applied to evaluate its ability to predict flow depths in open-channel junctions with transitional flows.

The observations were conducted in a 0.5 m wide, horizontal rectangular branch of which one side had a glass wall. Three angles of confluence, $\delta = 22.5°$, $\delta = 45°$, and $\delta = 90°$, were used. The width of each branch amounted to $B = 0.096$. The total flow discharge Q_d ranged between 0.002 and $0.013\,\mathrm{m}^3/\mathrm{s}$, and the upstream to downstream discharge ratio ranged between 0 and 1. Assuming critical flow at the entrance of the downstream branch leads to a Froude number equal to 1. Once a certain discharge Q_d was set, the discharge distribution could be varied to the desired

DOI: 10.1002/fld

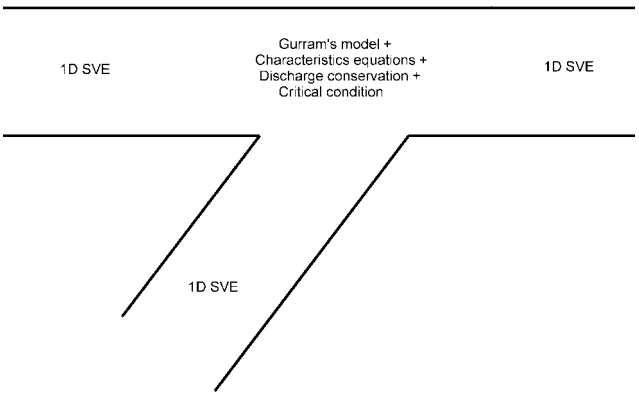

Figure 3. Treatment of the junction problem for the 1D case.

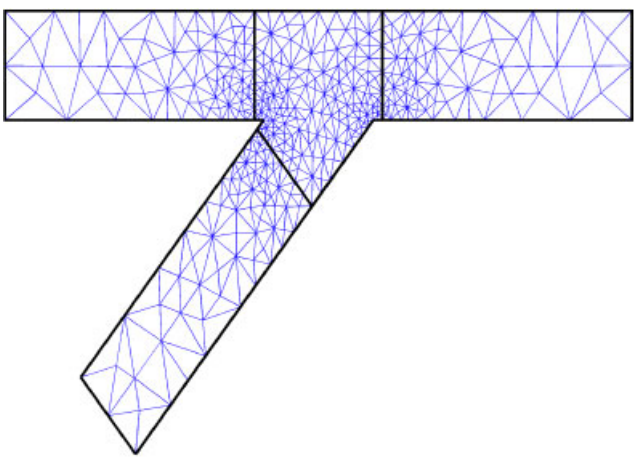

Figure 4. Definition of problem domain and the unstructured mesh for the 2D case.

value of q. The flow depths h_{u} and h_L were measured. It is found that the flow depths in the upstream and the lateral branches are nearly equal.

For the numerical simulation, flow discharges are fixed at the upstream branches and a free outfall condition is considered at the downstream branch, which makes waves pass the boundary without reflection. A free slip condition is applied at the solid boundary, i.e. the normal velocity component at the face is set to zero. The different flow parameters for the three angles (22.5, 45 and 90°) are listed in Tables I–III, respectively.

The study is organized around the prediction of the upstream to downstream depth ratio Y at the junction. Under a known upstream and lateral flow discharges, the upstream to downstream depth ratio Y is computed using the 1D approach and the 2D approach and compared with the experimental data of Hager [19].

DOI: 10.1002/fld

Table I. Flow parameters for the angle $\delta = 22.5°$.

Discharge ratio q	Main channel inflow Q_u (L/s)	Branch channel inflow Q_L (L/s)	Main channel outflow Q_d (L/s)
0	0	7.8	7.8
0.0493	0.3845	7.4155	7.8
0.0585	0.1170	1.8830	2
0.0905	0.7059	7.0941	7.8
0.1195	0.2390	1.7610	2
0.1423	1.1099	6.6901	7.8
0.1713	1.9956	9.6544	11.65
0.2124	1.6567	6.1433	7.8
0.2428	1.8938	5.9062	7.8
0.3219	2.5108	5.2892	7.8
0.3630	4.2289	7.4211	11.65
0.3918	3.0560	4.7440	7.8
0.4207	3.2815	4.5185	7.8
0.4436	5.1679	6.4821	11.65
0.4937	5.7516	5.8984	11.65
0.5363	1.0726	0.9274	2
0.6016	1.2032	0.7968	2
0.6441	7.5038	4.1462	11.65
0.6973	5.4389	2.3611	7.8
0.7337	8.5476	3.1024	11.65
0.7838	6.1136	1.6864	7.8
0.8338	6.5036	1.2964	7.8

Table II. Flow parameters for the angle $\delta = 45°$.

Discharge ratio q	Main channel inflow Q_u (L/s)	Branch channel inflow Q_L (L/s)	Main channel outflow Q_d (L/s)
0	0	4.9	4.9
0.0389	0.3034	7.4966	7.8
0.0694	0.5413	7.2587	7.8
0.1897	1.4797	6.3203	7.8
0.2779	2.1676	5.6324	7.8
0.3539	2.7604	5.0396	7.8
0.4633	3.6137	4.1863	7.8
0.5211	4.0646	3.7354	7.8
0.5591	1.1182	0.8818	2.0
0.6669	1.3338	0.6662	2.0
0.7140	1.4280	0.5720	2.0
0.7489	3.6696	1.2304	4.9
0.8141	3.9891	0.9109	4.9
0.8520	1.7040	0.2960	2.0
0.9141	7.1200	0.6700	7.8

DOI: 10.1002/fld

Table III. Flow parameters for the angle $\delta = 90°$.

Discharge ratio q	Main channel inflow Q_u (L/s)	Branch channel inflow Q_L (L/s)	Main channel outflow Q_d (L/s)
0	0	5.9	5.9
0.0780	0.6084	7.1916	7.8
0.0870	0.6786	7.1214	7.8
0.1053	0.8213	6.9787	7.8
0.2528	1.4915	4.4085	5.9
0.2664	2.0779	5.7221	7.8
0.4684	3.6535	4.1465	7.8
0.5033	2.9695	2.9305	5.9
0.7021	5.4764	2.3236	7.8
0.7521	4.4374	1.4626	5.9
0.8552	6.6706	1.1294	7.8
0.8824	6.8827	0.9173	7.8
0.9021	7.0364	0.7636	7.8
0.9444	7.3663	0.4337	7.8

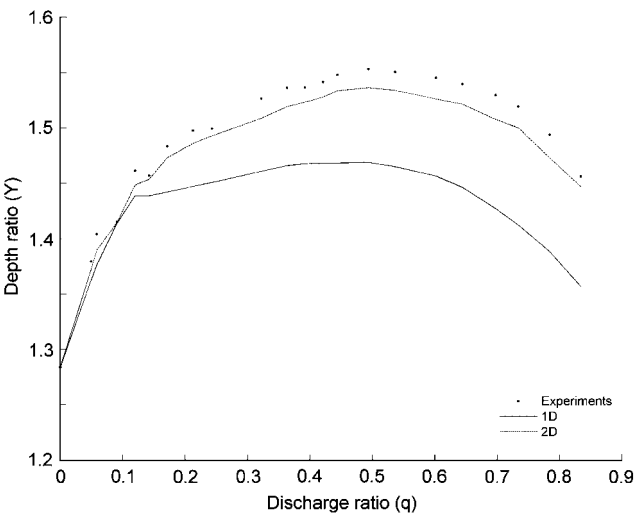

Figure 5. Comparison of water depth ratio Y as a function of the discharge flow ratio q for the junction angle ($\delta = 22.5°$).

Comparison between experimental data and numerical results obtained with the 1D approach and the 2D approach is shown. Figures 5–7 represent, respectively, the water depth ratios Y plotted against the discharge ratios for the three angles of intersection (22.5, 45 , and 90°) that Hirsh [8] investigated. Experimental results are well reproduced by the 2D approach. The figures indicate an excellent agreement between the experimental data and the results obtained by the 2D approach. The 2D approach's prediction correlates well to the measured data and gives better accuracy than

DOI: 10.1002/fld

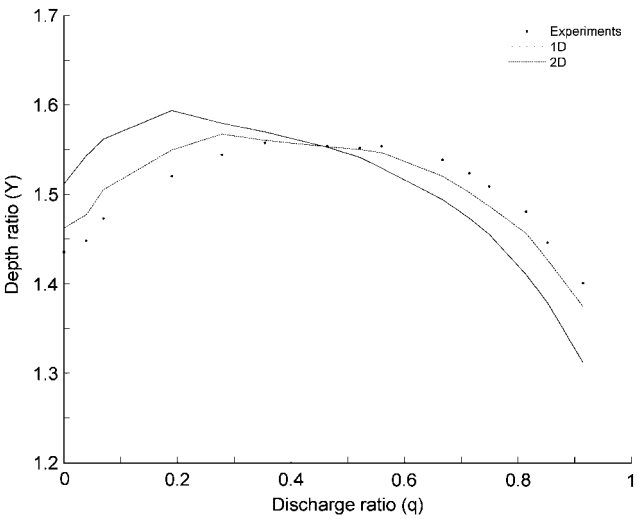

Figure 6. Comparison of water depth ratio Y as a function of the discharge flow ratio q for the junction angle ($\delta = 45°$).

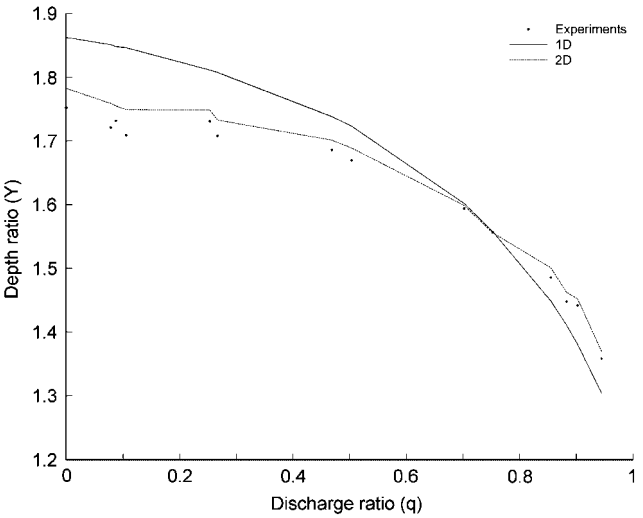

Figure 7. Comparison of water depth ratio Y as a function of the discharge flow ratio q for the junction angle ($\delta = 90°$).

the ones provided by the 1D approach, which does not always achieve a very good agreement. A notable deviation between the results obtained by the 1D approach and the experimental data is found.

DOI: 10.1002/fld

Table IV. Errors of the water depths as defined in Equation (25).

Angle (deg.)	1D error in %	2D error in %
$\delta = 22.5$	7.06	1.43
$\delta = 45$	6.55	2.19
$\delta = 90$	8.03	2.21

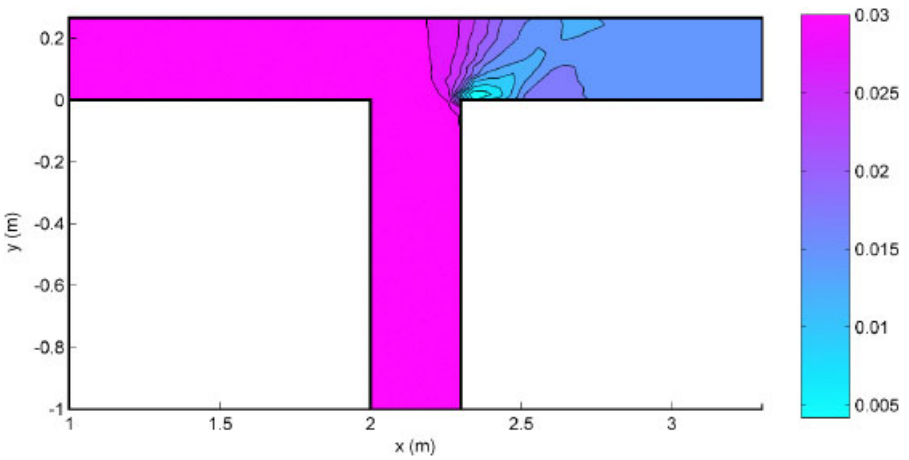

Figure 8. Contour of water depths in channel junction.

For a more accurate study of the water depth ratios' prediction, we introduce an estimator of quality defined as follows:

$$E = 100 \cdot \max \left| \frac{Y_{\mathrm{p}} - Y_{\mathrm{m}}}{\min(Y_{\mathrm{m}})} \right| \tag{25}$$

where Y_{p} and Y_{m} is the predicted and measured water depth ratios, respectively.

Table IV presents the errors as defined in Equation (25) between the measured data and the water depth ratio predicted by the two approaches 1D and 2D.

According to Table IV, and in all the investigated tests, the 2D approach gives the best agreement with the experimental data. The error of this approach is about 2% in all cases. Moreover, these good agreements were obtained with a reasonable effort. Whereas, the error with the 1D approach is not sufficiently acceptable and reaches 8%.

In spite of the fact that the computing time for the 2D approach is much more significant than for the 1D approach, the reasons of this choice are on the one hand the possibility of representing the different urban structures, and on the other hand, the 2D approach allows to directly calculate the flows in the junctions. Thus, they do not have recourse to additional empirical equations. Moreover, the results of the 2D calculations are more accurate and more informative.

The following example illustrates the 2D computational procedure of transitional flow at open-channel junction: Consider a junction of two channels at a confluence angle $\delta = 90°$. The upstream and lateral bottom slopes are $S_0 = 0.001$, the downstream bottom slope is $S_0 = 0.01$, and the

DOI: 10.1002/fld

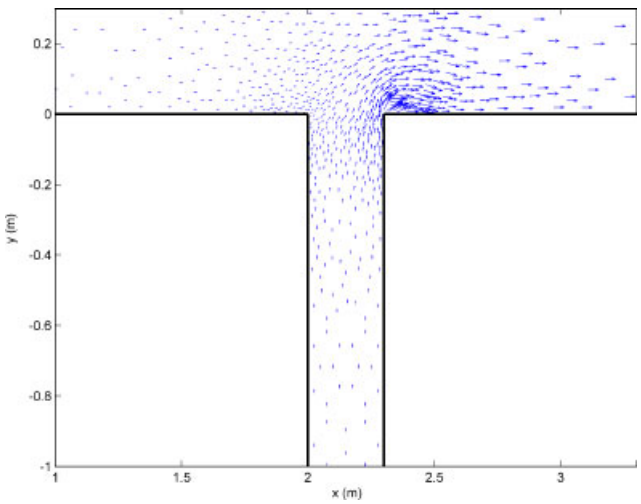

Figure 9. 2D ploy of velocity field in channel junction.

roughness coefficient according to Manning's formula amounts to 0.012. Find the upstream flow depths h_u and h_L for a downstream discharge $Q_d = 4$ L/s if the channels are $L = 2$ m length and $B = 0.3$ m wide, and the lateral discharge $Q_L = 2$ L/s.

The contour of water depths and the vectors of horizontal flow velocities are shown in Figures 8 and 9, respectively. The uniform flow depth in the downstream channel is $h_N = 0.0155$ m, whereas the critical flow depth is $h_c = [0.004^2/(9.81.0.3^2)]^{1/3} = 0.0263\,m > h_N$. Therefore, supercritical flow establishes in the downstream branch. In the upstream branches $h_N = 0.03\,m > h_c = 0.0165$ m, so subcritical flow takes place in the upstream branches. This example indicates that the following conditions are satisfied: subcritical inflow and supercritical flow immediately downstream of the junction. Therefore, transitional flow from subcritical flow in the upstream branches to supercritical flow in the downstream branch will be established as assumed.

6. CONCLUSION

In this study, a 1D and 2D approach has been applied for steady transitional flow at open-channel junction.

For the 1D study, the 1D Saint Venant equations coupled with the method of characteristics and a junction model based on momentum conservation are used to find the solution in the network system (branches and junction). While for the 2D case, the whole system is discretized into triangular cells forming an unstructured computational mesh. Therefore, we simply apply the 2D Saint Venant equations, which are solved by a second-order RKDG method. The numerical results have been validated by comparison with experimental data. In all the considered cases, the 2D approach gives the best agreement with respect to the experimental data. The 1D approach does not achieve a very good agreement, while the 2D approach performs almost well in all the cases and for the different junction angles that Hager had investigated. Moreover, these good agreements were obtained with a reasonable space discretization and therefore a reasonable CPU time.

DOI: 10.1002/fld

This work shows therefore that the idea of combining a 1D approach in branches to a 2D approach for the junctions in practical situation is fully satisfied when we observed the quality of the 2D simulation results. It is clear that in certain complex flows such as supercritical flow in which hydraulic jumps may occur, the coupling of the 1D and 2D models may not be so simple. Therefore, the use of TVD schemes with shock capturing when solving the 1D and 2D Saint Venant equations is necessary to correctly represent the hydraulic jumps. Future work will focus on this point and will consist of developing a framework based on coupling:

- The 1D Saint Venant equations to be applied in branches.
- The 2D Saint Venant equations to be applied at the junction area.

REFERENCES

1. Yen BC. *Unsteady Flow Mathematical Modeling Techniques*, *Modeling of Rivers*, Shen HW (ed.), vol. 13(1). Wiley Interscience: New York, 1979; 13–33.
2. Akan AO, Yen BC. Diffusion wave flood routing in channel network. *Journal of Hydraulic Division* 1981; **107**(6):719–723.
3. Yen BC, Osman A. Flood routing through river junctions. *ASCE Rivers '76*, vol. 1. New York, 1976; 212–231.
4. Gurram SK. A study of subcritical and transitional combining flow in open channel junctions. *Ph.D. Thesis*, Banaras Hindu University, Varanasi, India, 1994.
5. Cockburn B, Shu CW. The Runge–Kutta discontinuous Galerkin method for conservative laws V: multidimensional systems. *Journal of Computational Physics* 1998; **141**:199–224.
6. Schwanenberg D. Die Runge–Kutta discontinuous Galerkin Methode zur Losung konvektionsdominierter tiefengemittelter Flachwasserprobleme. *Ph.D. Thesis*, Aachen University, Germany, 2003.
7. Schwanenberg D, Harms M. Discontinuous Galerkin finite-element method for transcritical two-dimensional shallow water flows. *Journal of Hydraulic Engineering* 2004; **130**(5):412–421.
8. Hirsh C. *Numerical Computation of Internal and External Flows*. A Wiley Interscience Publication: New York, 1990.
9. Taylor EH. Flow characteristics at rectangular open-channel junctions. *Transactions* (ASCE) 1944; **109**:893–912.
10. Webber NB, Greated CA. An investigation of flow behaviour at the junction of rectangular channels. *Proceedings of the Institute of Civil Engineers*, London, vol. 34, 1966; 321–334.
11. Modi PN, Ariel PD, Dandekar MM. Conformal mapping for channel junction flow. *Journal of Hydraulic Division* 1981; **107**(12):1713–1733.
12. Best JL, Reid I. Separation zone at open-channel junctions. *Journal of Hydraulic Engineering* 1984; **110**(11): 1588–1594.
13. Hager WH. Discussion of 'Separation zone at open-channel junctions' by Best JL and Reid I. *Journal of Hydraulic Engineering* 1987; **113**(4):539–543.
14. Ramamurthy AS, Carballada LB, Tran DM. Combining open channel flow at right angled junctions. *Journal of Hydraulic Engineering* 1988; **114**(12):1449–1460.
15. Gurram SK, Karki KS, Hager WH. Subcritical junction flow. *Journal of Hydraulic Engineering* 1997; **123**(5): 447–455.
16. Hsu CC, Lee WJ, Chang CH. Subcritical open channel junction flow. *Journal of Hydraulic Engineering* 1998; **124**(8):847–855.
17. Hsu CC, Wu SF, Lee WJ. Flow at 90° equal-width open-channel junction. *Journal of Hydraulic Engineering* 1998; **124**(2):186–191.
18. Shabayek S, Steffler P, Hicks F. Dynamic model for subcritical combining flows in channel junctions. *Journal of Hydraulic Engineering* 2002; **128**(9):821–828.
19. Hager WH. Transitional flow in channel junctions. *Journal of Hydraulic Engineering* 1989; **115**(2):243–259.
20. Godunov S. Finite difference methods for numerical computation of discontinuous solutions of the equations of fluid dynamics. *Matematicheskii Sbornik* 1959; **47**:271–306.

DOI: 10.1002/fld